·神经影像学·

基于扩散加权成像的儿童后颅窝常见肿瘤诊断与鉴别诊断

丁兴华 祝迎锋 张超 祝翊倩 张荣

【摘要】 **目的** 探讨儿童后颅窝常见肿瘤的影像学诊断与鉴别诊断方法，并按照先定位诊断再定性诊断的思路，基于DWI是否弥散受限提出儿童后颅窝常见肿瘤的诊断流程图。**方法** 共纳入2021年1月至2024年1月在复旦大学附属华山医院予以手术切除的118例儿童后颅窝肿瘤患者，均行头部CT和MRI检查，并据此进行术前定位和定性诊断，分别以术中所见和术后病理学检查为诊断“金标准”，判断术前定位诊断和定性诊断的准确性；再基于DWI是否弥散受限提出儿童后颅窝常见肿瘤的诊断流程图。**结果** 共118例后颅窝肿瘤患儿定位和定性诊断为第四脑室肿瘤计41例，包括髓母细胞瘤27例、毛细胞型星形细胞瘤7例、室管膜瘤5例、脉络丛乳头状瘤1例、形成菊形团的胶质神经元肿瘤1例；脑干肿瘤38例，包括弥漫性中线胶质瘤，H3 K27变异型24例、毛细胞型星形细胞瘤5例、海绵状血管瘤3例、儿童型弥漫性高级别胶质瘤（倾向弥漫性中线胶质瘤，H3野生型）2例、节细胞胶质瘤2例、非典型性畸胎样/横纹肌样肿瘤1例、儿童型弥漫性低级别胶质瘤1例；脑桥小脑角肿瘤计9例，包括毛细胞型星形细胞瘤3例、胆脂瘤2例、髓母细胞瘤1例、弥漫性中线胶质瘤，H3 K27变异型1例、毛细胞黏液型星形细胞瘤1例、尤文肉瘤1例；小脑肿瘤计30例，包括毛细胞型星形细胞瘤15例、髓母细胞瘤7例、海绵状血管瘤2例、室管膜瘤1例、儿童型弥漫性低级别胶质瘤1例、儿童型弥漫性高级别胶质瘤（倾向弥漫性中线胶质瘤，H3野生型）1例、胚胎发育不良性神经上皮肿瘤1例、错构瘤1例和肾外横纹肌样瘤小脑转移瘤1例。定位诊断，术前CT的定位诊断准确率为93.22%（110/118），MRI的定位诊断准确率达100%（118/118）。定性诊断，74例（62.71%）患儿定性诊断准确，23例（19.49%）诊断笼统，21例（17.80%）诊断错误。儿童后颅窝肿瘤的影像学鉴别诊断集中于髓母细胞瘤、毛细胞型星形细胞瘤、室管膜瘤、弥漫性中线胶质瘤，H3 K27变异型。位于脑干外的髓母细胞瘤、毛细胞型星形细胞瘤和室管膜瘤的DWI弥散受限发生率分别为100%（35/35）、4%（1/25）和5/6，3种肿瘤之间差异有统计学意义（$Z=-5.601$，$P=0.000$）；位于脑干的弥漫性中线胶质瘤，H3 K27变异型和毛细胞型星形细胞瘤的DWI弥散受限发生率为79.17%（19/24）和1/5，两种肿瘤之间差异亦有统计学意义（Fisher确切概率法；$P=0.038$）。**结论** 儿童后颅窝肿瘤早期诊断较为困难，DWI是鉴别诊断的重要依据，基于DWI是否弥散受限提出的儿童后颅窝常见肿瘤诊断流程图有望提高术前诊断的准确性。

【关键词】 脑肿瘤； 颅窝，后； 磁共振成像； 诊断，鉴别； 儿童

Study on diagnosis and differential diagnosis of common tumors in the posterior fossa of children based on diffusion-weighted imaging

DING Xing-hua[1], ZHU Ying-feng[2], ZHANG Chao[1], ZHU Yi-qian[1], ZHANG Rong[1]

[1]Department of Neurosurgery, [2]Department of Pathology, Huashan Hospital, Fudan University, Shanghai 200040, China

Corresponding author: ZHANG Rong (Email: zhang_rong@msn.com)

【Abstract】 **Objective** To investigate the imaging diagnosis and differential diagnosis methods for common tumors in the posterior fossa of children, and to propose a flow chart for the diagnosis of common tumors in the posterior fossa of children based on the limited diffusion of DWI according to the idea of

doi：10.3969/j.issn.1672-6731.2024.09.006

基金项目：上海周良辅医学发展基金会（青年医生科研托举计划）资助（项目编号：XM00050-2024-3-6）

作者单位：200040 上海，复旦大学附属华山医院神经外科（丁兴华、张超、祝翊倩、张荣），病理科（祝迎锋）

通讯作者：张荣，Email：zhang_rong@msn.com

localization diagnosis followed by qualitative diagnosis. **Methods** A total of 118 pediatric patients with posterior fossa tumors who underwent surgical resection in Huashan Hospital, Fudan University from January 2021 to January 2024 were enrolled, and all of them underwent head CT and MRI examinations, and preoperative localization diagnosis and qualitative diagnosis were carried out accordingly. Then, based on whether DWI was diffusion limited, a flow chart for the diagnosis of common tumors in the posterior fossa of children was proposed. **Results** A total of 118 children with posterior fossa tumors were localization and qualitatively diagnosed, including 41 cases of fourth ventricular tumors, including medulloblastoma (27 cases), pilocytic astrocytoma (7 cases), ependymoma (5 cases), choroid plexus papilloma (one case), and rosette-forming glioneuronal tumor (RGNT, one case). There were 38 cases of brainstem tumors, including 24 cases of diffuse midline glioma, H3 K27-altered, 5 cases of pilocytic astrocytoma, 3 cases of cavernous hemangioma, 2 cases of pediatric-type diffuse high-grade glioma (prone to diffuse midline glioma, H3 wild type), 2 cases of ganglio glioma, one case of atypical teratoid/rhabdoid tumor (AT/RT), and one case of pediatric-type diffuse low-grade glioma. There were 9 cases of cerebellopontine angle (CPA) tumors, including 3 cases of pilocytic astrocytoma, 2 cases of cholesteatoma, one case of medulloblastoma, one case of diffuse midline glioma, H3 K27-altered, one case of pilomyxoid astrocytoma, and one case of Ewing sarcoma. There were 30 cases of cerebellar tumors, including 15 cases of pilocytic astrocytoma, 7 cases of medulloblastoma, 2 cases of cavernous hemangioma, one case of ependymoma, one case of pediatric-type diffuse low-grade glioma, one case of pediatric-type diffuse high-grade glioma (prone to diffuse midline glioma, H3 wild type), one case of dysembryoplastic neuroepithelial tumor (DNT), one case of hamartoma, and one case of extrarenal rhabdomyomatoid tumor cerebellar metastases. Localization diagnosis, the accuracy of preoperative CT was 93.22% (110/118), while the accuracy of preoperative MRI was 100% (118/118). Qualitative diagnosis, 74 cases (62.71%) had accurate qualitative diagnosis, 23 cases (19.49%) had general diagnosis, and 21 cases (17.80%) had wrong diagnosis. The imaging differential diagnosis of posterior fossa tumors in children focuses on medulloblastoma, pilocytic astrocytoma, ependymoma, and diffuse midline glioma, H3 K27-altered. The incidence of limited diffusion of DWI in medulloblastoma, pilocytic astrocytoma and ependymoma outside the brainstem was 100% (35/35), 4% (1/25) and 5/6, and the difference among the three tumors was statistically significant ($Z = -5.601$, $P = 0.000$). The incidence of limited diffusion of DWI in diffuse midline glioma, H3 K27-altered and pilocytic astrocytoma in the brainstem was 79.17% (19/24) and 1/5, and the difference between the two tumors was also statistically significant (Fisher's exact possibility: $P = 0.038$). **Conclusions** The early diagnosis of posterior fossa tumors in children is difficult, and DWI is an important basis for differential diagnosis.

【Key words】 Brain neoplasms; Cranial fossa, posterior; Magnetic resonance imaging; Diagnosis, differential; Child

This study was supported by Shanghai Zhou Liang-fu Medical Development Foundation (No. XM00050-2024-3-6).

Conflicts of interest: none declared

儿童后颅窝肿瘤指年龄≤14岁，位于小脑幕下、枕骨大孔上的肿瘤，包括髓母细胞瘤、毛细胞型星形细胞瘤、弥漫性中线胶质瘤、室管膜瘤、脉络丛乳头状瘤、海绵状血管瘤、节细胞胶质瘤、儿童型低级别胶质瘤、胆脂瘤、尤文肉瘤、错构瘤、转移瘤、血管母细胞瘤等十余种类型[1-2]。尽管后颅窝仅占颅内体积的10%，但有45%～60%的儿童脑肿瘤发生于此处[3]。由于后颅窝空间狭小，并且包含脑干、小脑、后组脑神经等重要结构，因此当后颅窝肿瘤体积较大时不仅引起较严重的临床症状，而且手术并发症发生率较高[4-6]。不同类型肿瘤的自然演变不同，治疗方法不同，临床结局亦不同，因此术前准确诊断至关重要，方可在此基础上实现儿童脑肿瘤的精准治疗。本研究以近3年在复旦大学附属华山医院予以手术切除的儿童后颅窝肿瘤患者为研究对象，回顾总结儿童后颅窝肿瘤的临床和影像学特点，探讨不同类型肿瘤的诊断与鉴别诊断方法，并按照先定位诊断再定性诊断的思路，提出儿童后颅窝肿瘤的诊断流程图，以为临床早期精确诊断提供帮助。

对象与方法

一、研究对象

1. 纳入与排除标准 （1）初发肿瘤且位于后颅

窝。(2)年龄≤14岁。(3)均予以手术切除并经术后病理学证实诊断。(4)排除肿瘤复发或二次手术、无法耐受手术或全身麻醉以及临床资料不完整的患儿。(5)所有患儿及其家属均对手术方案知情并签署知情同意书。

2.一般资料　选择2021年1月至2024年1月在复旦大学附属华山医院神经外科行手术切除的儿童后颅窝肿瘤患者共118例，男性70例，女性48例；年龄为2～14岁，平均(8.21±3.07)岁；病程7天至24个月，中位病程1.00(0.50，2.00)个月。13例为颅脑创伤后体检偶然发现，无临床症状；余105例的常见首发症状分别为头痛占36.19%(38/105)、呕吐占27.62%(29/105)、头晕占20.95%(22/105)、行走不稳占16.19%(17/105)、斜视占8.57%(9/105)，其中具有定位诊断意义的脑神经首发症状为面瘫3例(2.54%)，吞咽困难2例(1.69%)，面部麻木1例(0.85%)。

二、研究方法

1.术前头部影像学检查　(1)CT：术前均行头部CT扫描，观察肿瘤密度和边界、有无钙化或囊性变、有无幕上脑积水。(2)MRI：术前均行头部MRI扫描，包括DWI、表观扩散系数(ADC)和增强扫描。根据肿瘤组织与灰质的信号强度对比判断肿瘤是否弥散受限。增强扫描呈轻度强化、斑片状强化、团块状强化、条带状强化、明显强化、不均匀强化统一判定为肿瘤强化，无明显强化、未见明显增强、强化不明显统一判定为肿瘤无强化；对于囊实性肿瘤，以肿瘤实性部分强化程度判定肿瘤强化。

2.术前影像学诊断　(1)定位诊断：根据术前CT和MRI显示的肿瘤定位，肿瘤起源于小脑蚓，向第四脑室生长，或者主要占据第四脑室空间，定位诊断为第四脑室肿瘤；肿瘤起源于脑干或肿瘤主体位于脑干，定位诊断为脑干肿瘤；肿瘤起源于第四脑室侧孔，向一侧脑桥小脑角(CPA)生长，或者肿瘤主体位于脑桥小脑角，定位诊断为脑桥小脑角肿瘤；肿瘤起源于一侧小脑半球或肿瘤主体位于一侧小脑半球，定位诊断为小脑肿瘤。以术中实际所见为“金标准”，判断术前影像学定位诊断的准确性。(2)定性诊断：根据术前CT和MRI显示的肿瘤特征，对第四脑室肿瘤、脑干肿瘤、脑桥小脑角肿瘤和小脑肿瘤进行定性诊断。以术后病理学诊断为“金标准”，术前影像学定性诊断与术后病理学诊断完全一致判定为诊断准确，不一致判定为诊断错误，仅诊断某部位占位或者笼统诊断为胶质瘤而未区分儿童型高级别与低级别胶质瘤则判定为诊断笼统。

3.统计分析方法　采用SPSSAU数据科学分析平台(spssau.com/index.html)进行数据处理与分析。计数资料以相对数构成比(%)或率(%)表示，采用χ^2检验或Fisher确切概率法。呈正态分布的计量资料以均数±标准差($\bar{x}\pm s$)表示；呈非正态分布的计量资料以中位数和四分位数间距[$M(P_{25}，P_{75})$]表示，采用Mann-Whitney U检验。以$P\leq0.05$为差异具有统计学意义。

结　果

本研究118例后颅窝肿瘤患儿，经定位诊断和定性诊断分别为第四脑室肿瘤41例，包括髓母细胞瘤27例(图1)、毛细胞型星形细胞瘤7例、室管膜瘤5例(图2)、脉络丛乳头状瘤1例、形成菊形团的胶质神经元肿瘤(RGNT)1例；脑干肿瘤38例，包括弥漫性中线胶质瘤，H3 K27变异型24例(图3)、毛细胞型星形细胞瘤5例、海绵状血管瘤3例、儿童型弥漫性高级别胶质瘤(倾向弥漫性中线胶质瘤，H3野生型)2例、节细胞胶质瘤2例、非典型性畸胎样/横纹肌样肿瘤(AT/RT)1例、儿童型弥漫性低级别胶质瘤1例；脑桥小脑角肿瘤9例，包括毛细胞型星形细胞瘤3例、胆脂瘤2例、髓母细胞瘤1例、弥漫性中线胶质瘤，H3 K27变异型1例、毛细胞黏液型星形细胞瘤1例、尤文肉瘤1例；小脑肿瘤30例，包括毛细胞型星形细胞瘤15例(图4)、髓母细胞瘤7例(图5)、海绵状血管瘤2例、室管膜瘤1例、儿童型弥漫性低级别胶质瘤1例、儿童型弥漫性高级别胶质瘤(倾向弥漫性中线胶质瘤，H3野生型)1例、胚胎发育不良性神经上皮肿瘤(DNT)1例、错构瘤1例、肾外横纹肌样瘤小脑转移瘤1例。

定位诊断，术前CT的定位诊断准确率为93.22%(110/118)，8例小脑半球肿瘤分别误判为第四脑室肿瘤(3例)、脑干肿瘤(3例)和脑桥小脑角肿瘤(2例)；术前MRI的定位诊断准确率达100%(118/118)。定性诊断，74例(62.71%)诊断准确，23例(19.49%)诊断笼统，21例(17.80%)诊断错误，主要为髓母细胞瘤、毛细胞型星形细胞瘤、室管膜瘤三者之间的混淆18例，以及非典型性畸胎样/横纹肌样肿瘤误判为髓母细胞瘤1例，错构瘤误判为毛细胞型星形细胞瘤1例，脉络丛乳头状瘤误判为室管膜瘤1例。CT图像上，除胆脂瘤呈低密度外，其余

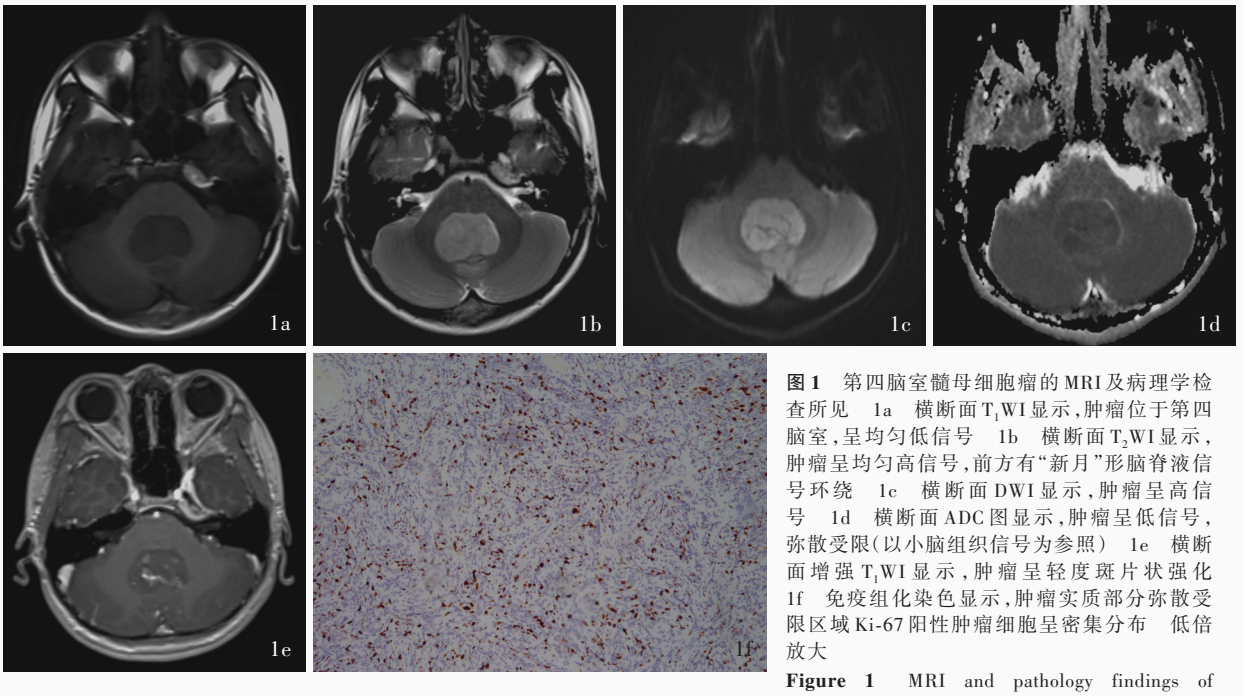

图1 第四脑室髓母细胞瘤的MRI及病理学检查所见 1a 横断面T_1WI显示，肿瘤位于第四脑室，呈均匀低信号 1b 横断面T_2WI显示，肿瘤呈均匀高信号，前方有“新月”形脑脊液信号环绕 1c 横断面DWI显示，肿瘤呈高信号 1d 横断面ADC图显示，肿瘤呈低信号，弥散受限（以小脑组织信号为参照） 1e 横断面增强T_1WI显示，肿瘤呈轻度斑片状强化 1f 免疫组化染色显示，肿瘤实质部分弥散受限区域Ki-67阳性肿瘤细胞呈密集分布 低倍放大

Figure 1 MRI and pathology findings of medulloblastoma in the fourth ventricle Axial T_1WI showed the tumor was located in the fourth ventricle and showed uniform hypointensity (Panel 1a). Axial T_2WI showed the tumor was uniformly hyperintense, and there was a "crescent" shaped cerebrospinal fluid (CSF) signal in front of the tumor (Panel 1b). Axial DWI showed the tumor was hyperintense (Panel 1c). Axial ADC showed the tumor was hypointense with limited diffusion (cerebellar tissue signal as reference, Panel 1d). Axial enhanced T_1WI showed the tumor was mildly patchy enhancement (Panel 1e). Immunohistochemical staining showed Ki-67 positive tumor cells were densely distributed in areas with limited diffusion of tumor parenchyma (Panel 1f). Low power magnified

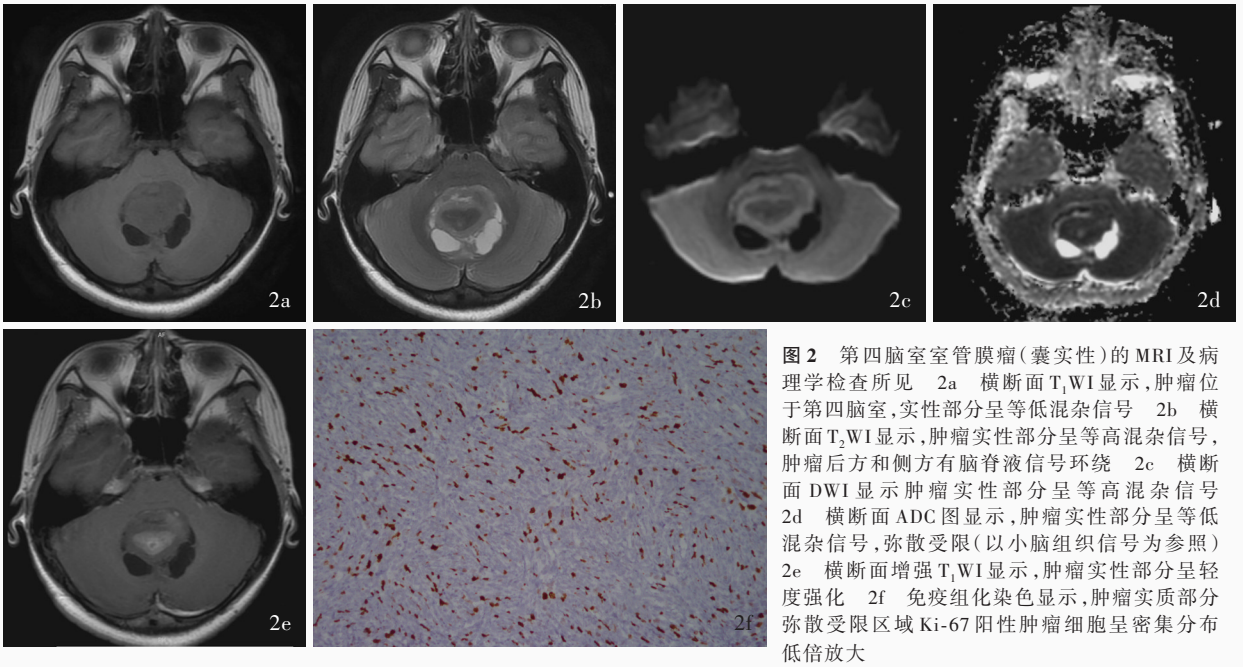

图2 第四脑室室管膜瘤（囊实性）的MRI及病理学检查所见 2a 横断面T_1WI显示，肿瘤位于第四脑室，实性部分呈等低混杂信号 2b 横断面T_2WI显示，肿瘤实性部分呈等高混杂信号，肿瘤后方和侧方有脑脊液信号环绕 2c 横断面DWI显示肿瘤实性部分呈等高混杂信号 2d 横断面ADC图显示，肿瘤实性部分呈等低混杂信号，弥散受限（以小脑组织信号为参照） 2e 横断面增强T_1WI显示，肿瘤实性部分呈轻度强化 2f 免疫组化染色显示，肿瘤实质部分弥散受限区域Ki-67阳性肿瘤细胞呈密集分布 低倍放大

Figure 2 MRI and pathology findings of ependymoma in the fourth ventricle (solid with cystic change) Axial T_1WI showed the tumor was located in the fourth ventricle, and the solid part showed a mixed signal of isointensity and hypointensity (Panel 2a). Axial T_2WI showed the solid part of the tumor was a mixed signal of isointensity and hyperintensity, and the CSF signal surrounded posterior and lateral of the tumor (Panel 2b). Axial DWI showed the solid part of the tumor showed a mixed signal of isointensity and hyperintensity (Panel 2c). Axial ADC showed a mixed signal of isointensity and hypointensity, with limited diffusion (cerebellar tissue signal as reference, Panel 2d). Axial enhanced T_1WI showed the solid part of the tumor was mild enhancement (Panel 2e). Immunohistochemical staining showed Ki-67 positive tumor cells were densely distributed in areas with limited diffusion of tumor parenchyma (Panel 2f). Low power magnified

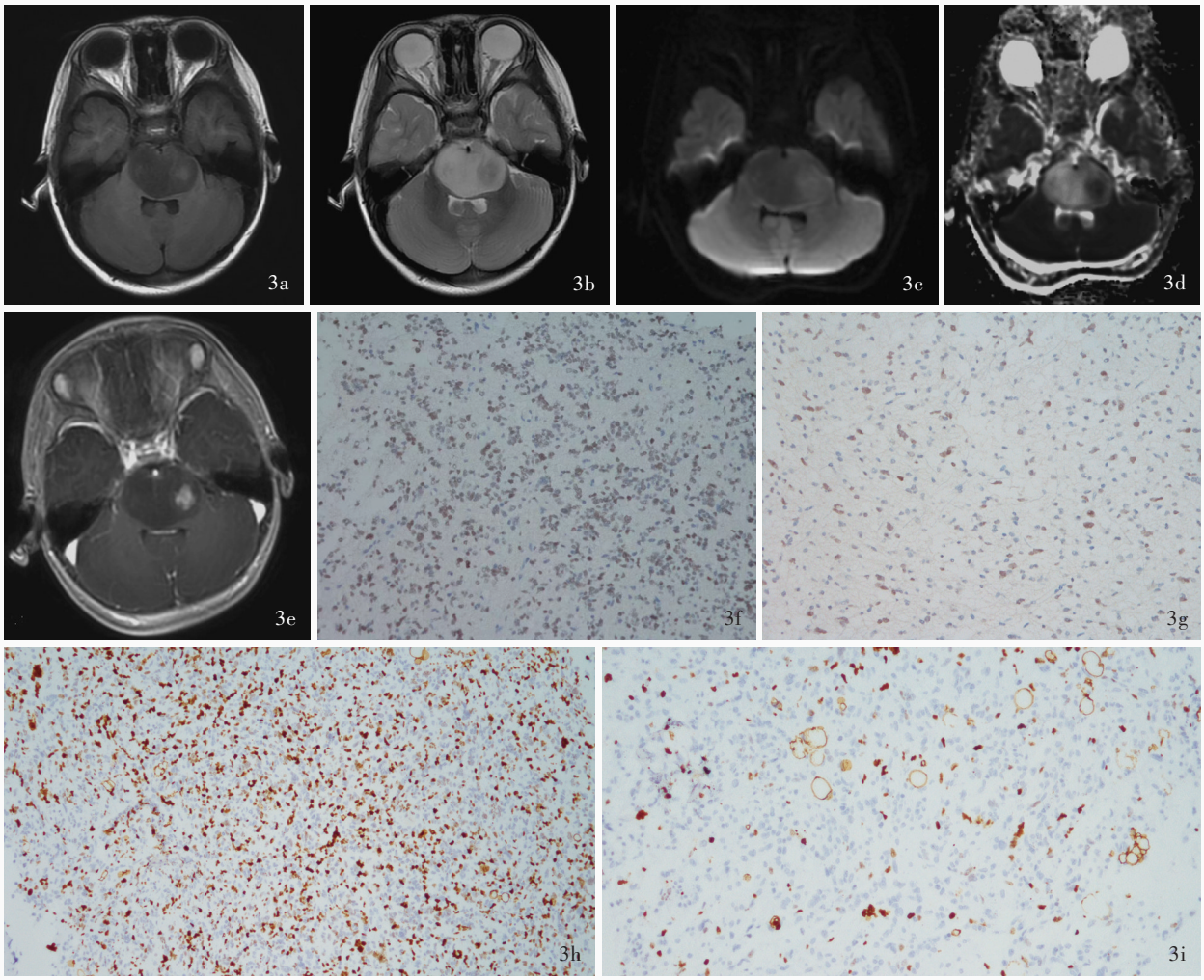

图3　弥漫性中线胶质瘤，H3 K27变异型的MRI及病理学检查所见　3a　横断面T_1WI显示，脑干弥漫性肿胀，呈低信号，病变左侧部分区域呈斑片状略高信号　3b　横断面T_2WI显示，脑干弥漫性肿胀，病变呈高信号并包绕基底动脉，病变左侧部分区域呈略高信号　3c　横断面DWI显示，病变左侧部分区域呈斑片状高信号　3d　横断面ADC显示，病变左侧部分区域呈低信号，弥散受限（以小脑组织信号为参照）　3e　横断面增强T_1WI显示，病变左侧部分区域呈明显强化，其余区域未见强化　3f，3g　免疫组化染色显示，肿瘤左侧弥散受限区域H3 K27M阳性肿瘤细胞呈密集分布，肿瘤左侧弥散不受限区域H3 K27M阳性肿瘤细胞呈稀疏分布　中倍放大　3h，3i　免疫组化染色显示，肿瘤左侧弥散受限区域Ki-67阳性肿瘤细胞呈密集分布，肿瘤左侧弥散不受限区域Ki-67阳性肿瘤细胞呈稀疏分布　低倍放大

Figure 3　MRI and pathology findings of diffuse midline glioma, H3 K27-altered　Axial T_1WI showed diffuse swelling of the brainstem with hypointensity, and patchy slightly hyperintensity in part of the left side of the lesion (Panel 3a). Axial T_2WI showed diffuse swelling of the brainstem with hyperintensity and surrounding the basilar artery, and slight hyperintensity in part of the left side (Panel 3b). Axial DWI showed patchy hyperintensity in part of the left side (Panel 3c). Axial ADC showed patchy hypointensity in part of the left side with limited diffusion (cerebellar tissue signal as reference, Panel 3d). Axial enhanced T_1WI showed that some areas on the left side was obvious enhancement, and most of the rest did not show enhancement (Panel 3e). Immunohistochemical staining showed dense distribution of H3 K27M-positive tumor cells in the left limited diffusion area (Panel 3f), and sparse distribution of H3 K27M-positive tumor cells in the left unlimited diffusion area (Panel 3g). Medium power magnified　Immunohistochemical staining showed dense distribution of Ki-67 positive tumor cells in the left limited diffusion area (Panel 3h), and sparse distribution of Ki-67 positive tumor cells in the left unlimited diffusion area (Panel 3i). Low power magnified

肿瘤均呈高低、等低混杂密度，无特异性；17例发生肿瘤钙化，分别为髓母细胞瘤9例（9/17）、毛细胞型星形细胞瘤5例（5/17）、室管膜瘤2例（2/17）、形成菊形团的胶质神经元肿瘤1例（1/17），各亚型肿瘤之间有无钙化差异无统计学意义（Fisher确切概率法：$P=0.241$），表明钙化不能作为区分髓母细胞瘤、毛细胞型星形细胞瘤、室管膜瘤与形成菊形团的胶质神经元肿瘤的依据。MRI图像上，海绵状血管瘤T_1WI和T_2WI呈“桑椹”状高低混杂信号，T_2WI病灶周围可见特征性低信号环，即含铁血黄素沉积带，多无强化征象；胆脂瘤好发于脑桥小脑角，明显弥散受限，亦无强化征象。因此，儿童后颅窝肿瘤的

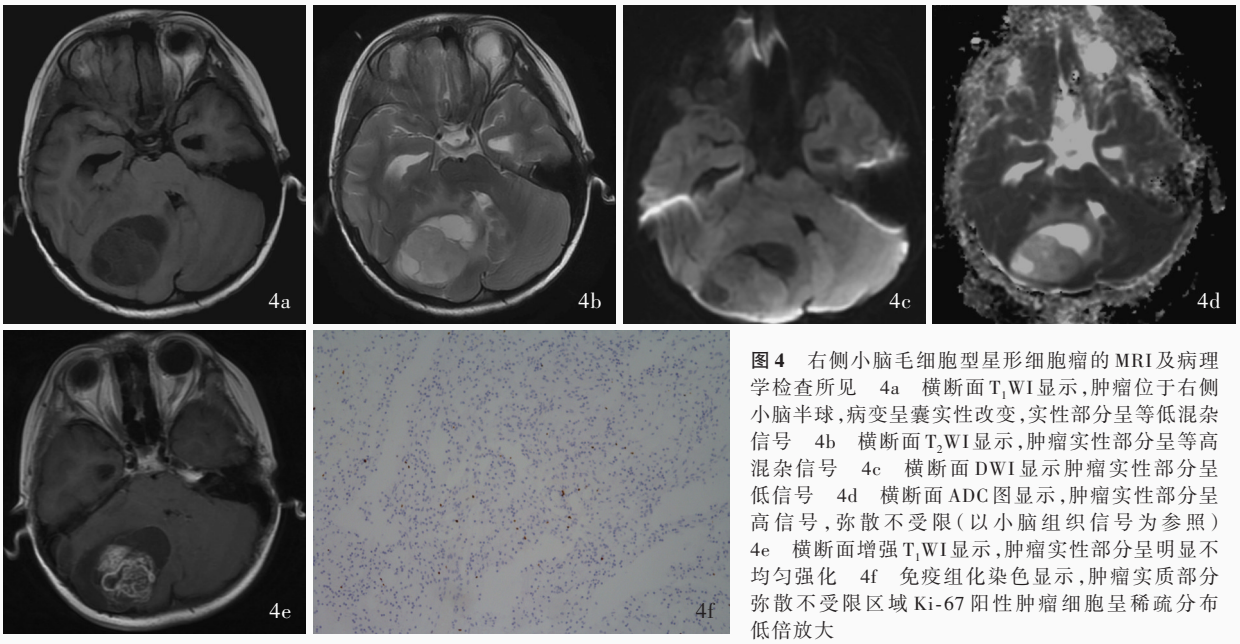

图4 右侧小脑毛细胞型星形细胞瘤的MRI及病理学检查所见 4a 横断面T_1WI显示，肿瘤位于右侧小脑半球，病变呈囊实性改变，实性部分呈等低混杂信号 4b 横断面T_2WI显示，肿瘤实性部分呈等高混杂信号 4c 横断面DWI显示肿瘤实性部分呈低信号 4d 横断面ADC图显示，肿瘤实性部分呈高信号，弥散不受限（以小脑组织信号为参照） 4e 横断面增强T_1WI显示，肿瘤实性部分呈明显不均匀强化 4f 免疫组化染色显示，肿瘤实质部分弥散不受限区域Ki-67阳性肿瘤细胞呈稀疏分布 低倍放大

Figure 4 MRI and pathology findings of pilocytic astrocytoma in right cerebellar Axial T_1WI showed the tumor was located in the right cerebellar hemisphere, and the lesion showed cystic solid changes, and the solid part showed a mixed signal of isointensity and hypointensity (Panel 4a). Axial T_2WI showed the solid part of the tumor showed a mixed signal of isointensity and hyperintensity (Panel 4b). Axial DWI showed hypointensity in the solid part of the tumor (Panel 4c). Axial ADC showed hyperintensity with unlimited diffusion (cerebellar tissue signal as a reference, Panel 4d). Axial enhanced T_1WI showed the solid part of the tumor was obvious uneven enhancement (Panel 4e). Immunohistochemical staining showed Ki-67 positive tumor cells were sparsely distributed in the unlimited diffusion area (Panel 4f). Low power magnified

影像学鉴别诊断主要集中于髓母细胞瘤、毛细胞型星形细胞瘤、室管膜瘤、弥漫性中线胶质瘤，H3 K27变异型，其中弥漫性中线胶质瘤，H3 K27变异型主要为脑干肿瘤。（1）髓母细胞瘤：肿瘤呈类圆形囊实性，边界较清晰，T_1WI呈等低混杂信号、T_2WI呈等高混杂信号且信号不均匀，瘤周水肿较轻，DWI呈高信号，ADC呈低信号，表现为部分区域弥散受限，增强扫描呈明显不均匀强化，囊性变区无明显强化（图1，5）。（2）毛细胞型星形细胞瘤：肿瘤呈囊实性，实性部分呈T_1WI低信号、T_2WI高信号，DWI表现为肿瘤实性部分呈低信号，ADC呈高信号，弥散不受限，增强扫描实性部分呈不均匀强化、囊壁不强化（图4）。（3）室管膜瘤：肿瘤呈囊实性，形态不规则，边界清晰，T_1WI呈等低混杂信号、T_2WI呈等高混杂信号，瘤周水肿不明显，DWI表现为肿瘤实性部分呈等高混杂信号，ADC呈等低混杂信号，部分区域弥散受限，增强扫描呈不均匀强化（图2）。（4）弥漫性中线胶质瘤，H3 K27变异型：肿瘤通常位于脑桥或延髓，T_1WI呈等或稍低信号、T_2WI呈等或稍高信号且多见“基底动脉包绕征”，多数DWI呈高信号，ADC呈低信号，部分区域弥散受限，增强扫描呈不均匀斑片状强化（图3）。不同类型肿瘤免疫组化染色显示，髓母细胞瘤、室管膜瘤的肿瘤细胞密集（图1f，2f，5f），毛细胞型星形细胞瘤的肿瘤细胞稀疏（图4f），弥漫性中线胶质瘤，H3 K27变异型弥散受限区域肿瘤细胞密集（图3f，3h），弥散不受限区域肿瘤细胞稀疏（图3g，3i），与MRI弥散受限表现相吻合。

本组患儿术前CT和MRI扫描显示肿瘤体积普遍较大，易压迫或堵塞第四脑室，出现梗阻性脑积水；位于脑干外的35例髓母细胞瘤、25例毛细胞型星形细胞瘤和6例室管膜瘤，梗阻性脑积水发生率分别为82.86%（29/35）、56%（14/25）和2/6，3种肿瘤之间差异有统计学意义（$P=0.004$）；DWI弥散受限发生率分别为100%（35/35）、4%（1/25）和5/6，3种肿瘤之间差异亦有统计学意义（$P=0.000$）；而囊性变发生率分别为20%（7/35）、40%（10/25）和1/6，3种肿瘤之间差异无统计学意义（$P=0.283$，表1）。

脑干肿瘤的鉴别诊断主要为弥漫性中线胶质瘤，H3 K27变异型与毛细胞型星形细胞瘤，二者病程分别为0.80（0.50，1.00）和2.00（0.60，5.00）个月，两种肿瘤之间差异无统计学意义（$P=0.104$）；囊性变发生率为8.33%（2/24）和0/5，两种肿瘤之间差异

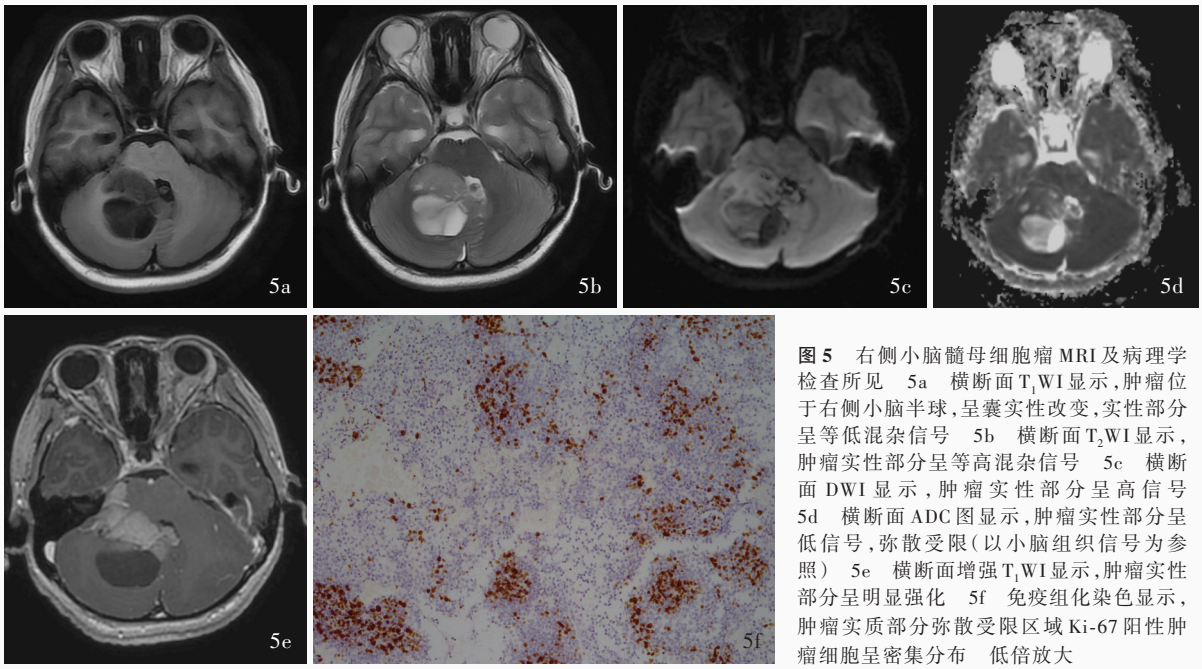

图5　右侧小脑髓母细胞瘤MRI及病理学检查所见　5a　横断面T_1WI显示，肿瘤位于右侧小脑半球，呈囊实性改变，实性部分呈等低混杂信号　5b　横断面T_2WI显示，肿瘤实性部分呈等高混杂信号　5c　横断面DWI显示，肿瘤实性部分呈高信号　5d　横断面ADC图显示，肿瘤实性部分呈低信号，弥散受限（以小脑组织信号为参照）　5e　横断面增强T_1WI显示，肿瘤实性部分呈明显强化　5f　免疫组化染色显示，肿瘤实质部分弥散受限区域Ki-67阳性肿瘤细胞呈密集分布　低倍放大

Figure 5　MRI and pathology findings of medulloblastoma in right cerebellar　Axial T_1WI showed the tumor was located in the right cerebellar hemisphere, showing cystic solid changes, and the solid part showed a mixed signal of isointensity and hypointensity (Panel 5a). Axial T_2WI showed a mixed signal of isointensity and hyperintensity in the solid part of the tumor (Panel 5b). Axial DWI showed hyperintensity in the solid part of the tumor (Panel 5c). Axial ADC showed hypointensity with limited diffusion (cerebellar tissue signal as a reference, Panel 5d). Axial enhanced T_1WI showed the solid part of the tumor was significant enhancement (Panel 5e). Immunohistochemical staining showed Ki-67 positive tumor cells were densely distributed in areas with limited diffusion of tumor parenchyma (Panel 5f).　Low power magnified

表1　位于脑干外的儿童后颅窝常见肿瘤DWI弥散受限、囊性变及梗阻性脑积水发生率的比较[例(%)]

Table 1.　Comparison of the incidence of limited diffusion of DWI, cystic changes and obstructive hydrocephalus in common posterior fossa tumors in children located outside the brainstem [case (%)]

组别	例数	DWI弥散受限	囊性变	梗阻性脑积水
髓母细胞瘤	35	35(100.00)	7(20.00)	29(82.86)
毛细胞型星形细胞瘤	25	1(　4.00)	10(40.00)	14(56.00)
室管膜瘤	6	5(5/6)	1(1/6)	2(2/6)
Z值		-5.601	-1.073	-2.878
P值		0.000	0.283	0.004

表2　儿童脑干常见肿瘤病程、DWI弥散受限、囊性变和强化发生率的比较

Table 2.　Comparison of duration, and incidence of limited diffusion of DWI, cystic changes and enhancement of common brainstem tumors in children

组别	例数	病程[$M(P_{25},P_{75})$,月]	DWI弥散受限[例(%)]	囊性变[例(%)]	强化[例(%)]
弥漫性中线胶质瘤，H3 K27变异型	24	0.80(0.50,1.00)	19(79.17)	2(8.33)	16(66.67)
毛细胞型星形细胞瘤	5	2.00(0.60,5.00)	1(1/5)	0(0/5)	1(1/5)
Z值		-1.625	—	—	—
P值		0.104	0.038	1.000	0.130

—，Fisher's exact probability，Fisher确切概率法

无统计学意义（Fisher确切概率法：P = 1.000）；强化发生率为66.67%（16/24）和1/5，两种肿瘤之间差异亦无统计学意义（Fisher确切概率法：P = 0.130）；而DWI弥散受限发生率为79.17%（19/24）和1/5，两种肿瘤之间差异有统计学意义（Fisher确切概率法：P = 0.038，表2）。

讨　论

由于儿童后颅窝肿瘤患者无法准确描述自身症状，特别是低龄患儿，颅骨尚未发育完全，颅缝易分离，早期可一定程度缓解颅内高压，往往脑积水和颅内高压已经很严重，但患儿并无剧烈头痛主诉，导致早期诊断困难。因此临床实践中，患儿反复出现无法解释的头痛、呕吐、头晕，即使症状不甚严重也应行头部CT筛查，发现可疑病灶即行头部MRI平扫和增强扫描以定位和定性诊断肿瘤[7]。本研究术前CT和MRI均显示肿瘤体积较大，仅11.86%（14/118）肿瘤最大径＜3 cm，表明即使影像

学涌现出诸多新方法，由于患儿无法准确描述自身症状，在肿瘤体积较小时，儿童后颅窝肿瘤的早期明确诊断仍较困难。

弥散受限指在某些特殊病理生理学过程中，如肿瘤细胞密度增加、体积增大致细胞外间隙减少或胞质内大分子含量增多等，水分子自由运动受到限制。DWI的工作原理是在T_2WI中加入运动敏感梯度脉冲以反映不同组织水分子弥散速度差异所产生的信号变化[8]。b值可反映这种运动敏感梯度强度，b值越大、运动敏感梯度越强、水分子弥散的影响越明显，b1000图像即为常见的DWI图像，但b1000图像显示某病灶为高信号时，并不能立即判断其弥散受限，也可能由该组织在T_2WI上呈高信号所引起，称为穿透效应[9]；同样的，b1000图像呈低信号也不一定提示弥散不受限，可能是由于病灶在T_2WI上信号较低而抵消弥散受限带来的高信号，称为暗化效应。如果b1000图像呈高信号、对应的ADC图像呈低信号，则提示弥散受限；如果b1000图像呈低信号、对应的ADC图像呈高信号，则提示弥散不受限[10]。

髓母细胞瘤、室管膜瘤、弥漫性中线胶质瘤，H3 K27变异型的恶性程度均较高，肿瘤细胞排列紧密，细胞外间隙水分子运动空间受限，加之肿瘤细胞核较大，细胞内水分子运动空间亦受限，因此上述3种肿瘤DWI呈高信号、ADC呈低信号，表现为弥散受限[11-12]。但对于同样位于第四脑室的髓母细胞瘤和室管膜瘤，均可能发生囊性变或钙化，DWI亦表现为弥散受限，鉴别诊断困难。有研究采用肿瘤组织/正常脑组织ADC比值对儿童后颅窝肿瘤进行鉴别诊断，ADC比值＞1.87为毛细胞型星形细胞瘤、1.19～1.87为室管膜瘤、＜1.19为髓母细胞瘤[13]，但是由于操作繁琐且可靠性存在争议，并未在临床推广应用。

髓母细胞瘤可伴钙化和瘤周水肿，MRI表现为T_1WI低信号、T_2WI高信号、FLAIR成像高信号，增强扫描呈明显均匀强化，边界较清晰，可伴囊性成分或坏死，可发生脑室系统内肿瘤播散，发生于脑脊液流动途径。室管膜瘤通常位于第四脑室或其周围，CT密度不均匀，瘤内钙化是较常见的征象；MRI表现为T_1WI等低混杂信号，这是由于肿瘤含有不同成分，如坏死、出血和囊性变，导致信号异质性，T_2WI高信号，这是由于肿瘤含水量较高，特别是囊性变或坏死区域，增强扫描呈明显强化征象，特别是肿瘤边缘或内部分隔处，表明肿瘤富含血管。髓母细胞瘤通常起源于后髓帆原始胚胎残留，向第四脑室生长，故常位于第四脑室顶部，肿瘤前方和上方可见“新月”形脑脊液信号、后方则无脑脊液信号；室管膜瘤通常起源于第四脑室底部室管膜，肿瘤后方和侧方常有脑脊液信号环绕、前方与脑干分界不清[14]，因此认为，横断面T_2WI显示肿瘤前方有脑脊液信号环绕时考虑髓母细胞瘤，后方有脑脊液信号环绕时考虑室管膜瘤，但是本研究由于室管膜瘤患儿例数偏少，未进行统计学分析。弥漫性中线胶质瘤，H3 K27变异型是儿童和青少年常见的恶性肿瘤，主要发生于脑干（如延髓、中脑或脑桥）、丘脑，尽管采用放射治疗和药物化疗等方法，患儿中位生存期仍较短（仅9～12个月），由于肿瘤位置深在及其浸润性，无法手术切除，有学者认为可根据术前影像学诊断直接放射治疗[15]。位于脑干的弥漫性中线胶质瘤CT表现为以脑桥为中心的低密度占位性病变，偶有囊性成分；MRI表现为T_1WI呈低信号，T_2WI和FLAIR成像呈高信号，肿瘤前部延伸通常包绕基底动脉，增强扫描呈不均匀、轻至中度强化，DWI表现为较高的弥散受限信号，表明肿瘤细胞密度较高。虽然影像学特征对诊断十分重要，但最终诊断依靠病理学检查，H3 K27M突变是弥漫性中线胶质瘤的重要分子标志物（图3f，3g）。位于后颅窝的毛细胞型星形细胞瘤好发于小脑半球和脑干，CT呈低密度，常伴有轻度瘤周水肿；T_1WI呈低或等信号，T_2WI和FLAIR成像呈高信号，增强扫描呈明显均匀强化，边界清晰；部分可能有囊性成分，囊内常含液体，T_2WI呈高信号，但是由于肿瘤细胞密度较低，DWI常表现为弥散不受限[16]。毛细胞型星形细胞瘤为WHO 1级的偏良性胶质瘤，肿瘤生长缓慢，病程较长，临床表现缺乏特异性，与其他后颅窝占位性病变一样，表现为头痛、头晕、呕吐、行走不稳等症状。

由此可见，传统的T_1WI、T_2WI、FLAIR成像和增强扫描对儿童后颅窝肿瘤的诊断以及评估肿瘤部位、大小和受累脑组织必不可少，但针对肿瘤类型可提供的信息有限。基于文献报道的DWI在儿童后颅窝肿瘤鉴别诊断中的作用[17-18]，本研究通过回顾总结髓母细胞瘤、毛细胞型星形细胞瘤、室管膜瘤和弥漫性中线胶质瘤的临床和影像学特点，按照先定位诊断再定性诊断的思路并结合文献，再经统计学分析，基于DWI是否弥散受限提出儿童后颅窝

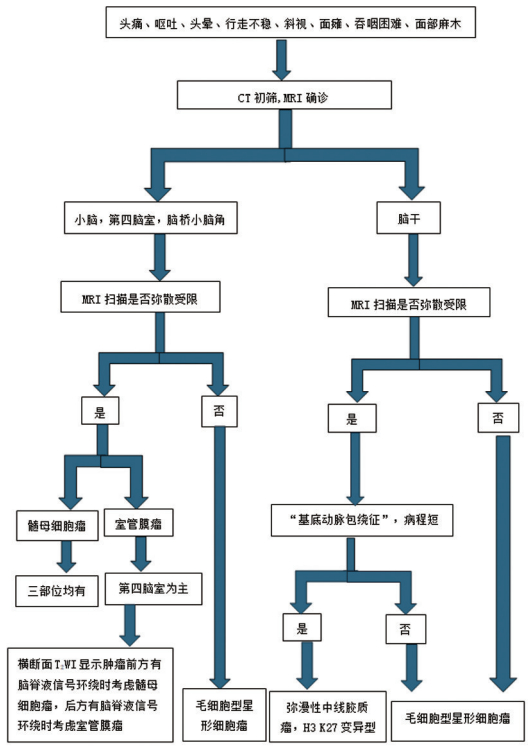

图6　儿童后颅窝肿瘤的诊断流程图

Figure 6　Diagnostic flow chart of posterior fossa tumors in children.

常见肿瘤的诊断流程图(图6),尚待大样本前瞻性研究进一步证实。

利益冲突　无

参　考　文　献

[1] Sun CR, Xu JH, Zhang BY, Xu SS, Dong F, Wei BX, Jiang B, Zhang JM. Interpretation on pediatric-type diffuse gliomas in the 2021 WHO Classification of Tumors of the Central Nervous System (fifth edition)[J]. Zhongguo Xian Dai Shen Jing Ji Bing Za Zhi, 2021, 21:791-803.[孙崇然, 许晶虹, 张布衣, 许素素, 董飞, 卫博星, 蒋飚, 张建民. 2021年世界卫生组织中枢神经系统肿瘤分类(第五版)儿童型弥漫性胶质瘤分类解读[J]. 中国现代神经疾病杂志, 2021, 21:791-803.]

[2] Totapally BR, Shah AH, Niazi T. Epidemiology and short-term surgical outcomes of children presenting with cerebellar tumors [J]. Clin Neurol Neurosurg, 2018, 168:97-101.

[3] Formentin C, Joaquim AF, Ghizoni E. Posterior fossa tumors in children: current insights[J]. Eur J Pediatr, 2023, 182:4833-4850.

[4] Mei F, Qiu RW, Mai YY, Chen SX, Liu SJ, Min XD, Yin ZH, Bao Y, Qi ST. History, status and prospect of pediatric brain tumors[J]. Zhongguo Xian Dai Shen Jing Ji Bing Za Zhi, 2020, 20:258-262.[梅芬, 邱若薇, 麦益颖, 陈舒娴, 刘思洁, 闵旭东, 尹铸豪, 包赟, 漆松涛. 儿童脑肿瘤治疗历史、现状及展望[J]. 中国现代神经疾病杂志, 2020, 20:258-262.]

[5] Chen ZR, Wan F, Li YK, Xu Y, Dong FY, Lei T. Clinical and pathological features of infant and young children brain tumors: single center report of 100 cases[J]. Zhongguo Xian Dai Shen Jing Ji Bing Za Zhi, 2019, 19:969-974.[陈籽荣, 万锋, 厉亚坤, 徐钰, 董芳永, 雷霆. 婴幼儿脑肿瘤临床及病理学特点:单中心100例分析[J]. 中国现代神经疾病杂志, 2019, 19:969-974.]

[6] Shi YX, Ma WB, Wang Y. Summary and analysis of clinical features and prognosis in pediatric gliomas based on the SEER database[J]. Zhongguo Xian Dai Shen Jing Ji Bing Za Zhi, 2021, 21:147-155.[石易鑫, 马文斌, 王裕. 基于美国SEER数据库的儿童胶质瘤临床特点和预后分析[J]. 中国现代神经疾病杂志, 2021, 21:147-155.]

[7] D'Arco F, Khan F, Mankad K, Ganau M, Caro-Dominguez P, Bisdas S. Differential diagnosis of posterior fossa tumours in children: new insights[J]. Pediatr Radiol, 2018, 48:1955-1963.

[8] Hao DP, Xu WJ, Xu AD. Basic principles and clinical application progress of MR diffusion-weighted imaging [J]. Zhongguo Zhong Xi Yi Jie He Ying Xiang Xue Za Zhi, 2003, 1: 244-247.[郝大鹏, 徐文坚, 徐爱德. MR弥散加权成像基本原理及临床应用进展[J]. 中国中西医结合影像学杂志, 2003, 1: 244-247.]

[9] Su WT, Pan ZL, Xu JC, Song RB, Rao M. Investigation and solution for T2 shine-through effects in MR diffusion-weighted imaging[J]. Zhongguo Yi Xue Ji Suan Ji Cheng Xiang Za Zhi, 2015, 21:219-223.[苏文婷, 潘自来, 徐敬慈, 宋瑞波, 饶敏. 磁共振弥散成像中T2穿透效应的影响及解决方法研究[J]. 中国医学计算机成像杂志, 2015, 21:219-223.]

[10] Li X, Zhang YK. Several related concepts and image interpretation in diffusion-weighted imaging[J]. Zhongguo Zu Zhong Za Zhi, 2022, 17:195-199.[李昕, 张英魁. 扩散加权成像中几个相关概念与图像解读[J]. 中国卒中杂志, 2022, 17: 195-199.]

[11] Chen L, Liu M, Bao J, Xia Y, Zhang J, Zhang L, Huang X, Wang J. The correlation between apparent diffusion coefficient and tumor cellularity in patients: a meta-analysis[J]. PLoS One, 2013, 8:e79008.

[12] Rodriguez Gutierrez D, Awwad A, Meijer L, Manita M, Jaspan T, Dineen RA, Grundy RG, Auer DP. Metrics and textural features of MRI diffusion to improve classification of pediatric posterior fossa tumors[J]. AJNR Am J Neuroradiol, 2014, 35: 1009-1015.

[13] Deng XL, Wen M, Wu XF, Ge XD, Li ML. Differential diagnosis of pediatric posterior fossa tumors using apparent diffusion coefficient ratios[J]. Zhongguo Yi Xue Ying Xiang Ji Shu, 2015, 31:1620-1624.[邓小林, 文明, 吴晓凤, 葛晓东, 李姝玲. ADC比值鉴别诊断儿童后颅窝肿瘤[J]. 中国医学影像技术, 2015, 31:1620-1624.]

[14] Poretti A, Meoded A, Huisman TA. Neuroimaging of pediatric posterior fossa tumors including review of the literature[J]. J Magn Reson Imaging, 2012, 35:32-47.

[15] Guarnera A, Romano A, Moltoni G, Ius T, Palizzi S, Romano A, Bagatto D, Minniti G, Bozzao A. The role of advanced MRI sequences in the diagnosis and follow-up of adult brainstem gliomas: a neuroradiological review[J]. Tomography, 2023, 9: 1526-1537.

[16] Ma Y, Li XG, Huang J, Kang HY, Zhang WG. Functional magnetic resonance imaging of pilocytic astrocytoma[J]. Zhongguo Yi Xue Ying Xiang Xue Za Zhi, 2015, 23:423-427.[马芸, 李晓光, 黄杰, 康厚艺, 张伟国. 毛细胞型星形细胞瘤的功能MRI表现[J]. 中国医学影像学杂志, 2015, 23:423-427.]

[17] Brandão LA, Young Poussaint T. Posterior fossa tumors [J]. Neuroimaging Clin N Am, 2017, 27:1-37.

[18] Mengide JP, Berros MF, Turza ME, Liñares JM. Posterior fossa tumors in children: an update and new concepts[J]. Surg Neurol Int, 2023, 14:114.

(收稿日期:2024-08-01)
(本文编辑:彭一帆)